Quantifying Human and Environmental Impacts on Land Use Patterns in the Yellow River Delta

Inam Ullah[1], Weidong Li[1,*], Sheheryar[2], Zhenying Li[1]

[1]College of information Science and Engineering, Henan University of Technology, Zhengzhou, Henan, China
[2]College of Water Conservancy, North China University of Water Resources & Electric Power, Zhengzhou, Henan, China
*Corresponding author: Weidong Li

Abstract: The Yellow River Delta (YRD) in Shandong Province, China, is a critical economic region that has undergone substantial land use/land cover (LULC) changes due to rapid development and populace growth over recent decades. This study seeks to examine the spatial variations in LULC changes and to identify the factors that influence these transitions in the YRD. We used the Random Forest (RF) cataloging approach on the Google Earth Engine (GEE) framework, with Landsat TM/OLI satellite images. Additionally, the driving influences behind these changes were analyzed using the Factor Indicator within the Geodetector framework, offering insights into the key influences on LULC dynamics. Our findings reveal significant variations in the dominant land use categories in the YRD. Agricultural land has decreased from 71.30% to 56.59%, while urban land has expanded from 7.89% to 23.09%. The Factor Detector analysis highlights population growth, Gross Domestic Product (GDP), temperature, and rainfall as the primary drivers behind these land use alterations. These results provide essential data to guide environmental protection efforts and support sustainable development in the YRD, assisting local governments in balancing socio-economic growth with ecological preservation.

Keywords: Land use Land Change (LULC); Google Earth Engine (GEE); Landsat TM/OLI Data; Random Forest (RF) Classification; Remote Sensing.

1. Introduction

Land serves as a critical foundation for human survival and advancement, offering vital perspectives on the interactions between human endeavors and ecological dynamics. LULC, discernible through multi-temporal observational data, indicates shifts in land utilization strategies [1]. Since the onset of the 21st century, the study of LULC changes has increasingly become a focal point in global environmental change research. Initiatives spearheaded by programs such as the Global Geosphere-Biosphere Project (IGBP) and the Interagency Human Determinants Project (IHDP) have positioned LULC changes at the forefront of scientific inquiry in this domain [2]. Amidst ongoing global socio-economic development, these alterations in LULC are expected to exacerbate, thereby exerting substantial pressures on ecosystem structures, functions, and the delivery of ecosystem services [3]. Thus, examining LULC changes provides an essential methodical origin for fostering sustainable and equitable progress among area economies and the natural atmosphere.

Remote detecting knowledge delivers a highly effective means for monitoring LULC, characterized by its extensive reach, frequent updates, and rich data provision [4]. This method has been the focus of numerous research creativities. Notably, the Global Geosphere-Biosphere Programme and the US Geological Inquiry have collaboratively formed a comprehensive worldwide LULC dataset, which offers a resolution of 1 km utilizing Enhanced Extremely Superior Resolution Radiometer data. In a specific study, Stefanski and colleagues employed Landsat and ERS SAR imagery coupled with the Random Forest method to delineate LULC in the west part of Ukraine over the period from 1986 to 2010 [5]. Similarly, Souza investigated the dynamics of LULC in Brazil spanning from 1985 to 2017 through the analysis of Landsat imagery. Furthermore, Abdullah utilized both XGBoost and random forest algorithms to assess LULC trends in coastal Bangladesh from 1990 to 2017 [6]. Collectively, these studies underscore the robust aptitudes of remote sensing technologies in the extraction and analysis of LULC data.

The swift progress in cloud storag and computing technologies has facilitated the growth of remote-detecting cloud stages that streamline the downloading and dispensation of substantial datasets. GEE, a prominent cloud-based platform, specializes in the analysis of worldwide scale Earth opinion data. This platform consolidates further than 200 datasets, including those from Sentinel, Landsat, and MODIS, providing a comprehensive resource for geospatial analysis. GEE supports both JavaScript and Python environments, empowering users to manage and process data on a petabyte scale efficiently. By offering tools for querying, visualization, preprocessing, and data extraction, GEE markedly alleviates the operational burden on remote sensing professionals.

Analyzing the driving influences of LULC change is essential for optimizing models and improving LULC

efficiency. Current methods of analysis are divided into qualitative and quantitative approaches. Qualitative methods identify the impacts of factors on LULC change but cannot quantify their influence [7]. Conversely, quantitative methods can measure these impacts but fail to capture the spatial relationships between factors and LULC changes, hindering a comprehensive empathetic of the underlying mechanisms. The geographic indicator, a statistical technique based on spatial distinction, overcomes these limitations by quantifying the impact of driving influences and analyzing their spatial interactions [8]. This method has been effectively applied in LULC research to investigate factors influencing specific changes, such as urban expansion, and vegetation cover dynamics.

Amidst swift socio-economic growth and urban expansion, coupled with natural sedimentation and uplift, the YRD has emerged as one of China's most vibrant regions. Although some scholars have explored changes in land cover within the YRD, contemporary research on this topic remains scarce. Previous investigations have predominantly concentrated on spatial analyses of rivers and urban areas, offering a scant quantitative examination of land use transformations across the region.

This manuscript seeks to examine changes in LULC within the YRD by analyzing long-term trends. Employing the GEE cloud stage coupled with the random forest cataloging algorithm, this study extracted and assessed LULC data from 2000, 2010, and 2020 for the YRD region. The intensity of land use was quantitatively measured and visually depicted through grid-based spatial representations, facilitating an analysis of its sequential and spatial fluctuations.

This paper comprehensively explores the spatial and sequential dynamics of various land use categories, and also analyzes the driving influences in the YRD, thereby providing a theoretical basis and practical references for the maintainable management of land capital and environmental protection in the YRD.

2. Materials and methods

The section presents a concise overview of the methodologies used to investigate LULC changes in our study range. We begin by characterizing the study area's geographical, ecological, and socio-economic attributes. The data preparation process is then explained, involving careful handling of anthropogenic and natural datasets for enhanced accuracy and relevance. We also detail the creation of a multidimensional classification feature set designed to categorize land use effectively and describe the selection process for training and validation samples to ensure typicality and statistical validity. Finally, we explicate the methods used in the study, covering both the analytical techniques and the statistical tools employed to interpret the data.

2.1 Study Area

The YRD (117˚31' - 119˚18'E, 36˚55' - 38˚16'N), positioned within the silty fan region designed by sedimentary deposits from the Yellow River lower Lijin County in Shandong Jurisdiction, extends over an area of roughly 6,783 square kilometers. This delta is fan-shaped with Lijin County at its apex; it is bounded by the Tuhai River inlet to the north, the Xiaoqing River to the south, and encompasses Dongying City at its center. The landscape of the delta is predominantly flat, characterized by an average elevation below 10 meters. Situated in a mid-latitude region within a warm temperate zone, the delta is exposed to a warm temperate semi-humid continental downpour climate, influenced by both the Eurasian landmass and the Pacific Ocean. Figure 1 illustrates the geographical position of the research range.

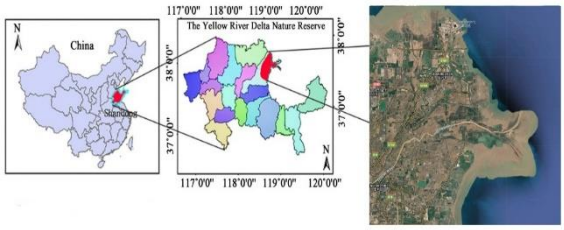

Figure 1. Map Depicting the Geographical Location of the Research Area

2.2 Establishing Data

The primary sources of data for this study include Landsat TM/OLI remote sensing imagery, essential geographic information, and socio-financial data sets. In the preprocessing phase, the study employs various techniques such as clarifying, cloud covering, mosaicking, and cropping on the Landsat TM/OLI data sets for the YRD. These operations are executed using the JavaScript Tender Programming Edge (API) on the framework of GEE. Subsequently, heights, gradients, and aspect data are derivative from the Digital Elevation Model (DEM).

Furthermore, various factors were identified to examine the spatial discrepancy features of LULC changes within the designated study zone, as detailed in Table 1.

Table 1. Influences of the LULC Type Changes

Influences type	Index	Code
Social Factor	Population	S1
	GDP	S2
Natural Factors	Temperature	N1
	Rain-fall	N2
	Elevation	N3
	Slope	N4
	Aspect	N5
	Soil	N6

These factors include population, GDP, temperature, precipitation, elevation, slope, aspect, and soil type. The relevant data obtained from data center of the Chinese Academy of Sciences and National Earth System Science Data Center. The dataset is accessible online at the following URLs: https://www.resdc.cn/, http://www.geodata.cn/.

2.2.1 Building multidimensional cataloging feature set

Leveraging the capabilities of the GEE platform, this research utilized the Landsat TM/OLI apparent reflectance datasets for the selected study range across the years 2000, 2010, and 2020. However, the region's complex climatic

conditions rendered the production of a cloud-free composite image from data collected in a single year unfeasible, introducing certain analytical constraints. To mitigate this, the study constructed a remote sensing image dataset for each target year by amalgamating all accessible images from the period of April to October. Thus, enhancing the quality of the classification.

The study computed Indices such as"the Normalized Difference Vegetation Index (NDVI) [9], Normalized Difference Developed Index (NDBI) [10], Enhanced Vegetation Index (EVI) [11], Normalized Difference Water Index (NDWI) [12], and Modified Normalized Difference Water Index (MNDWI) [13], and incorporated additional geographic variables—elevation, slope, and aspect—derivative from Digital Elevation Model (DEM) data. This integration aimed to augment the accuracy of classifications. Employing this methodology facilitated the generation of a comprehensive, high-quality feature set, which was effectively utilized for classification via the RF algorithm.

2.2.2 Training and authentication sample assortment

The cataloging of LULC types within the research location was derived from the existing LULC data, as well as pertinent literature sources. Within the area under investigation, LULC was branded into seven distinct types: cropland, forest land, water, bare ground, and urban land as revealed in Table 2.

When utilizing the RF algorithm for feature classification, it is imperative to use high-quality training and authentication samples. For this study, tasters from three distinct periods were collected through visual clarification of high-determination historical metaphors sourced from Google Earth Pro. Specifically, the sample sizes for the years 2000, 2010, and 2020 were 1470, 1451, and 1401, respectively. Of these, 70% of the sample points were allocated for training the classifiers, while the remaining 30% were used as validation tasters to verify the precision of the classifications.

Table 2. Land-use Categories Classified in the Study

LULC Type	Sub-type
Crop Land	Corn, wheat, rice, Mangroves, soy, fallow plots of structured land
Forest Land	Trees, clusters, plantations, grass fields, swamp
Water	River, lake, reservoir, pond
Bare Land	Exposed rock or soil, coastal tidal flat, dried lake beds
Urban Land	Construction, villages, cities, paved roads

2.2.3 Anthropogenetic and natural data

Our study used geo-detectors to assess the impact of many variables inside the chosen study region in order to look into the driving forces underlying changes in LULC. Essential variables such as density of population, GDP, altitude, aspect, climate, and rainfall were classified into six discrete categories using the natural breakpoint classification technique.

2.3 Methods

This work examines the taking out of LULC categories and the underlying drivers of LULC transformation in the YRD, utilizing multi-temporal Landsat sequence remote detecting imagery processed on the framework of the GEE. The methodological flow diagram is presented in Figure 2. Initially, the Landsat TM/OLI data were preprocessed through a series of steps, including information clarifying, cloud covering, tapestrying, and extracting on the GEE platform. Subsequently, the relevant property constraints were computed to generate a multidimensional cataloging property dataset. The RF procedure was then utilized to catalogue the LULC, with the cataloging accuracy assessed via a misperception matrix. Three distinct LULC cataloging products for the study range were obtained for the years 2000 to 2020. An allocation matrix was utilized to examine the fluctuations over time in each category of LULC. Lastly, the study investigated the LULC changes from the dual viewpoints of natural and social influences, employing earthly enquiries for driving force examination.

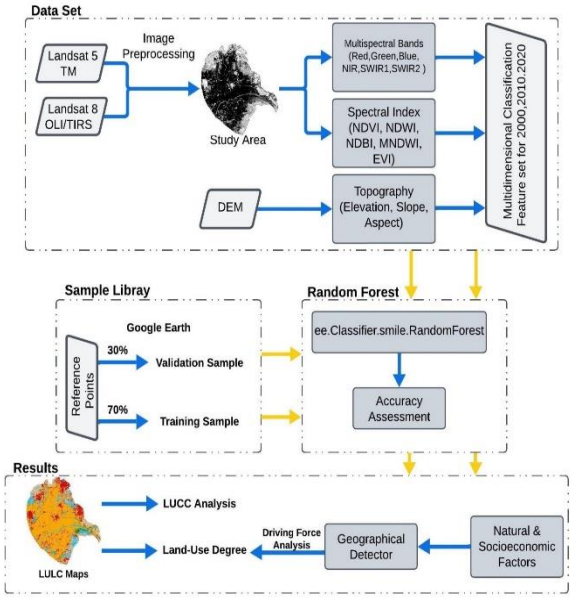

Figure 2. Flow Illustration of the Proposed Methodology

2.3.1 Trimming and correction

The early phase intricates obtaining the Landsat TM/OLI data for each year within the study area spanning 2000, 2010, and 2020. We utilized the GEE platform for denoising and correcting the Landsat TM/OLI data for each year. In accumulation, GEE raster cropping was employed to eliminate any background noise. Subsequently, we extracted the Landsat TM/OLI data specific to YRD for each year by employing the YRD managerial division map as a mask.

For the image cataloging method, we pragmatic a Random forest-supervised tagging algorithm.

2.3.2 Random forest algorithm

The RF procedure was applied to the LULC tagging, a combinatorial cataloging technique grounded on definite deterioration trees introduced by [14]. The core concept of

this procedure involves constructing an ensemble of verdict tree classifiers. Each decision tree provides a cataloging outcome, and the final cataloging is determined through a majority elective mechanism, which mitigates the risk of overfitting typically associated with individual decision trees. Compared to other machine erudition approaches, the RF algorithm demonstrates superior heftiness and performs efficiently on huge datasets [15]. Several studies have explored the use of the RF procedure for LULC cataloging on the GEE framework, yielding notable results.

The LULC classification was conducted by straight invoking the *ee.smileRandomForest* purpose within the GEE API. This function requires the specification of two limits: the amount of cataloging trees and the amount of characteristics parameters used during node splitting. Experimental results indicated that the classification accuracy was optimized when the quantity of trees was set to 500. Therefore, 500 trees were designated for the RF cataloging. Additionally, the amount of property variables was determined by calculating the square measure of the total amount of traits intricate in the cataloging process [16].

2.3.3 Evaluation

In this script, we employed a misperception matrix to assess the precision of cataloging outcomes for features within the study range. The precision of these cataloging results is further characterized through the calculation of overall precision, Kappa coefficient, fabricator's precision, and manipulator's precision.

a. Overall precision

The overall precision indicates the algorithm's efficacy and is quantified as the ratio of properly classified tasters to the total number of authentication tasters.

$$P_{OA} = \frac{1}{N}\sum_{i=1}^{n} \rho ii \quad (1)$$

In Equation 1, P_{OA} represents the general precision, N signifies the entire numeral of tasters utilized for the precision appraisal, n symbolizes the entire number of classes, and p_{ii} indicates the count of correctly classified instances for the i_{th} category in the muddle matrices.

b. The kappa coefficient

It quantifies the grade of a contract among observed ground fact information and projected values, accounting for agreement occurring by chance.

$$K = \frac{N\sum_{k=1}^{n} p_{kk} - \sum_{k=1}^{n}(\sum_{i=1}^{n} p_{ki}\sum_{j}^{n} p_{kj})}{N^2 - \sum_{k=1}^{n}(\sum_{i=1}^{n} p_{ki}\sum_{j=1}^{n} p_{kj})} \quad (2)$$

In Equation 2, K signifies the kappa coefficient; n signifies the total amount of groups; and p_{kk} signifies the numeral of accurate groupings for the k_{th} taster within the misperception matrix. The terms $\sum_{i=1}^{n} p_{ki}$ and $\sum_{j=1}^{n} p_{kj}$ correspond to the taster size in the i_{th} and j_{th} columns, correspondingly. N signifies the entire numeral of tasters utilized for precision assessment.

c. Producers precision

The drawing precision reflects the possibility that the ground certainty orientation data, represented by authentication samples, is accurately classified within the intended category.

$$P_{PA} = \frac{p_{kk}}{\sum_{j=1}^{n} p_{kj}} \quad (3)$$

In Equation 3, P_{PA} represents the mapping precision, n represents the entire numeral of classes, p_{kk} indicates the count of correctly classified instances for the k_{th} category in the disarray matrix, and $\sum_{j=1}^{n} p_{kj}$ signifies the taster size in the j_{th} section.

d. Users accuracy

User precision denotes the amount of accurately categorized pixels within a designated class relative to the entire pixel count in same group across the subsection.

$$P_{UA} = \frac{p_{kk}}{\sum_{i=1}^{n} p_{ki}} \quad (4)$$

In Equation 4, P_{UA} represents user precision; n represents the total amount of groups; p_{kk} signifies the count of precise arrangements for the k_{th} taster within the misperception matrix; and $\sum_{i=1}^{n} p_{ki}$ signifies the i_{th} line taster size.

2.3.4 Land use degree indices

This study evaluates the catalogue of land use level within the YRD by employing the complex land use directory, which acts as a measure of the extent of human activities on land. The extent of occupancy and growth within the area fundamentally determines these indices. A developed worth signifies a greater grade of occupancy, reflecting further intricate social and financial events within the range [17]. The computation of the land use grade in the research range is as below:

$$l_a = 100 \times \sum_{i=1}^{n} A_i \times C_i \quad (5)$$

The land use pattern index value is denoted as l_a, where A_i represents the land use classifying catalog, and C_i corresponds to the proportion of the range classified under the i_{th} land use degree. Based on appropriate revisions [18], the land use categories were categorized into four separate modules, each assigned a corresponding grading index, as detailed in *Table 3*.

Table 3. Land Reserve use Categories and Rankings

Type of Land	LULC Type	Index of Classification
Barren Land	Bare Land (costal tidal flat & deserts)	1
Natural Land	Forest Land, Water Body	2
Farming Land	Crop Land	3
Construction Land	Urban Land	4

2.3.5 Dominant factor detection

The Geodetector methodology evolved by combining Geographic Information System (GIS) technology, temporal overlay methods, and ensemble theory, based on the principles of spatial variation [19]. This method offers a novel approach to identifying the driving factors behind spatial differentiation, addressing the limitations of traditional mathematical-statistical models, which typically rely on numerous expectations and extensive data necessities [20]. The Geographical Detector comprises four distinct indicators: the influence indicator, interaction indicator, peril indicator, and environmental indicator. This script identifies the determinants of LULC variation

within the study range, in accordance with the research's objectives.

The influence indicator is primarily employed to assess the spatial array of the depending variable and the descriptive authority of the sovereign mutable about the reliance on the mutable. This study quantifies the descriptive authority of the impact of X_i on the geographically varied appearances of land use alteration [21]. The explanatory power, denoted as q, can be stated as:

$$q = 1 - \frac{\sum_{h=1}^{L} N_h \sigma_h^2}{N\sigma^2} \quad (6)$$

Let L represent the variety of coats of the sovereign mutable, N and N_h denote the number of tasters underneath each respective coat and area, and σ^2 indicate the overall variation of the taster.

3. Results

The upcoming sections of this article will delve into various aspects of LULC analysis. *Accuracy Valuation* will evaluate the precision of the land use data and its reliability. *LULC Structure Change* will analyze the shifts in land use patterns over time. Section *Transition Area Analysis of Land Use Type* will explore areas where land use types are transitioning, highlighting the factors influencing these changes. *Land Use Degree Changes* will examine the extent to which land use has transformed. Lastly, *Single Factor Detection Analysis* will focus on identifying and evaluating the impact of individual factors contributing to land use changes.

3.1 Accuracy Valuation

The accuracy of cataloging outcomes is a crucial component in LULC change examination. This study premeditated the misperception matrix for the training tasters and cataloging outcomes for each year using the GEE framework. *Table 1*, *Table 2*, and *Table 3*, presented the outcomes, show that the general classification precision for 2000, 2010, and 2020 was 79.2%, 77.6%, and 78.5%, correspondingly, while the kappa coefficients for these years were 0.79, 0.77, and 0.78, correspondingly. The overall precision and kappa coefficient for cataloging during the three stages exceeded 78%, with dissimilar LULC categories demonstrating high cartographic precision across the cataloging results for each date. Therefore, it can be decided that the overall cataloging precision met a satisfactory threshold, confirming that the cataloging results are both precise and consistent. To further evaluate the precision of the cataloging outcomes, numerous segments of the classified grades within the study range were randomly selected and subsequently compared with data from Google Earth Pro. As illustrated in *Figure 2*, the cataloging results presented in this study demonstrated an improved ability to distinguish crop land, forest land, water body, bare land, and urban land. These classifications exhibited a strong resemblance with the features observed in Google Earth Pro imagery. General, the findings of this study confirm the accuracy and reliability of the LULC classifications.

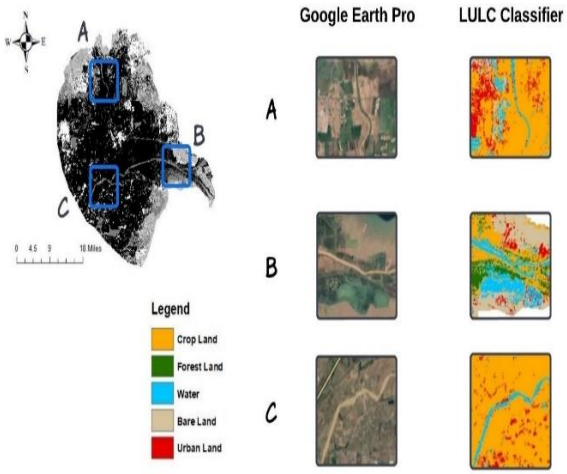

Figure 2. Typical Image Subsections (A-C) with their Cataloging Results

Table 1. The Results of Accuracy Assessment (2000)

LULC Type	2000	
	P_{UA}(%)	P_{PA} (%)
Crop Land	79.1	78.6
Forest Land	80.2	79.3
Water	78.7	70.1
Bare Land	73.1	72.4
Urban Land	70.5	79.2
P_{OA}(%)	79.2	
Kappa Coefficient	0.79	

Table 2. The Results of Accuracy Assessment (2010)

LULC Type	2010	
	P_{UA}(%)	P_{PA} (%)
Crop Land	81.3	79.3
Forest Land	78.4	80.2
Water	80.3	71.4
Bare Land	75.5	73.7
Urban Land	72.3	71.2
P_{OA}(%)	77.6	
Kappa Coefficient	0.77	

Table 3. The Results of Accuracy Assessment (2020)

LULC Type	2020	
	P_{UA}(%)	P_{PA} (%)
Crop Land	80.0	79.2
Forest Land	79.2	78.1
Water	72.4	73.3
Bare Land	73.2	75.5
Urban Land	77.1	78.1
P_{OA}(%)	78.5	
Kappa Coefficient	0.78	

3.2 Change in LULC Structure

The geographical dispersal of LUCC in the YRD in the years 2000, 2010, and 2020 is presented in *Figure 4* and *Figure 5*.

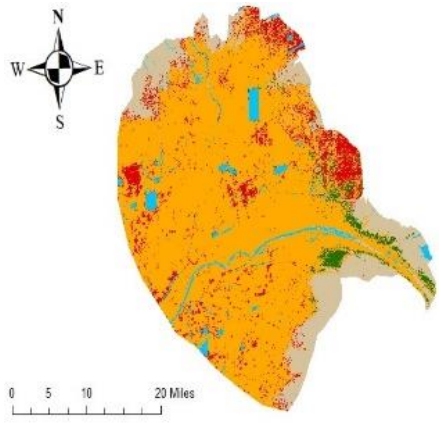

(a). 2000

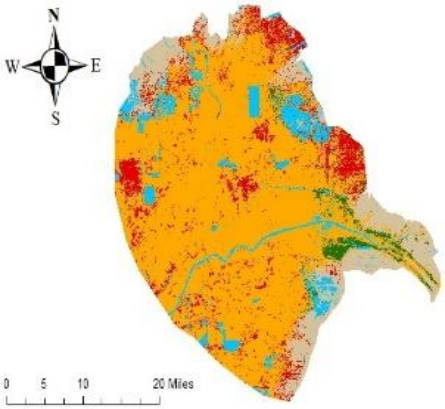

(b). 2010

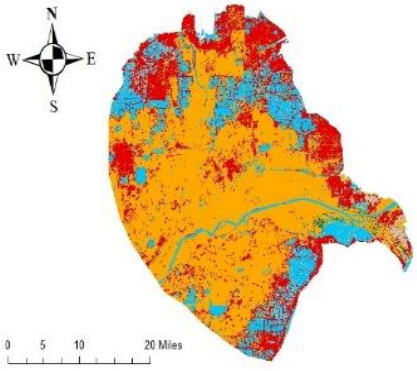

(c). 2020

Figure 4. Geographical Dispensation Map of LULC in the YRD, (a) 2000; (b) 2010; (c) 2020

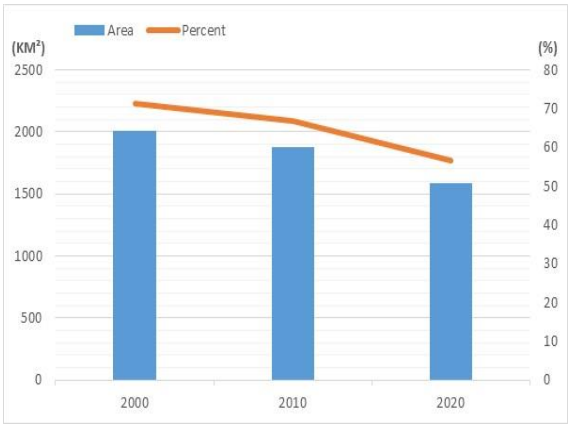

(a). Crop Land

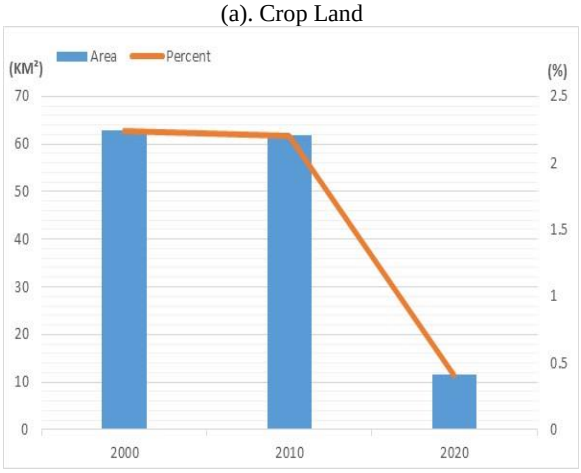

(b). Forest Land

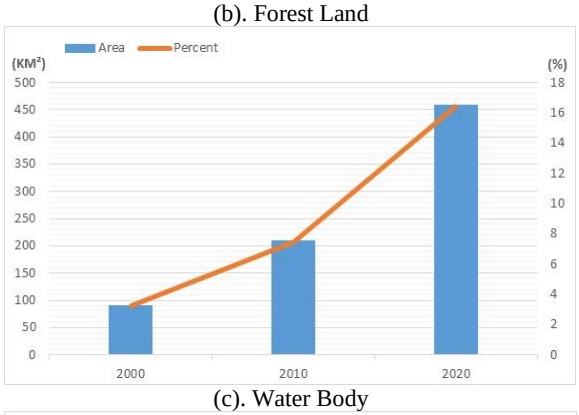

(c). Water Body

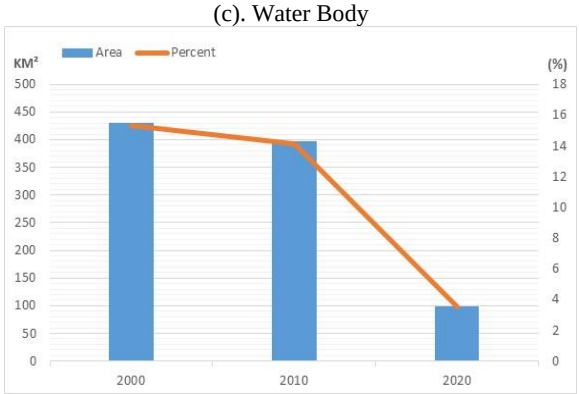

(d). Bare Land

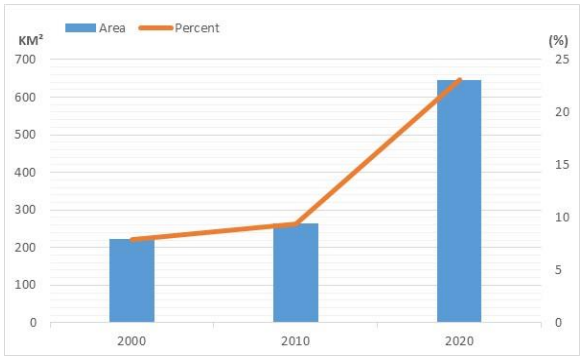

(e). Urban Land

Figure 5. Area Changes of LULC Categories, (a) Crop Land; (b) Forest Land; (c) Water Body; (d) Bare Land; (e) Urban Land

As depicted, crops dominate the LULC categories within the study range, covering over 2004.95 km ²in 2000, 1879.05 km ² in 2010, and 1583.34 km ² in 2020, which shows that the crops land decreased rapidly in the YRD from 2000 to 2020. The area of forested land has also shown a gradual decrease from 62.75 km ²in 2000, 61.79 in 2010, and 11.61 in 2020, which proves that the forest land faced a massive decrease from 2010 to 2020. The extent of bare ground has decreased, as built-up cover has expanded through both natural regeneration and human-driven efforts. Urbanization has accelerated significantly, with the built-up area expanding rapidly due to industrial development and infrastructure projects in coastal regions. Urban sprawl has grown from 221.96 km ²in 2000, 264.04 km ² in 2010 to 646.18 km ² in 2020, particularly around industrial zones, ports, and transportation hubs, resulting in the alteration of agricultural and natural land into urbanized areas. Table 7 provides a numerical depiction of the area of various types of LULC.

Table 7. Area of Various Types

Years	2000	2010	2020
Crop Land (Km^2)	2004.8	1879.0	1583.3
Forest Land (Km^2)	62.7	61.79	11.6
Water Body (Km^2)	91.1	209.5	458.4
Bare Land (Km^2)	430.9	397.4	98.1
Urban Land (Km^2)	221.9	264.0	646.1

3.3 Change Area Analysis of Land Use Type

To accurately and intuitively illustrate the quantifiable structural features and the change relationships among diverse LULC categories, we computed the LULC transfer matrix for the YRD. This matrix quantitatively delineates the mutual changes among various LULC types within the region. The total transfer matrices for LULC types from 2000 to 2010 and from 2010 to 2020 are shown in Table 8 and Table 9. In overall, the areas of urban land and water bodies in the research range have pointedly improved, while the ranges of cropland, forest land, and bare land have reduced.

Table 8. Transition Matrix of LULC (2000-2010)

LULC Type	Total Area in 2000	Total Area in 2010
Crop Land (Km^2)	2004.8	1879.0
Forest Land (Km^2)	62.7	61.7
Water (Km^2)	91.1	209.5
Bare Land (Km^2)	430.9	397.4
Urban Land (Km^2)	221.96	264.04

Table 4. Transition Matrix of LULC (2010-2020)

LULC Type	Total Area in 2010	Total Area in 2020
Crop Land (Km^2)	1879.0	1583.3
Forest Land (Km^2)	61.7	11.6
Water (Km^2)	209.5	458.4
Bare Land (Km^2)	397.4	98.1
Urban Land (Km^2)	264.0	646.1

Regarding the major land use/land cover (LULC) transitions, the evolution of urban land mostly happened at the expenditure of cropland, whereas the reduction in bare land primarily transitioned to water bodies and urban land. Between 2010 and 2020, the urban land and water bodies continued to expand, while bare land and forest land exhibited a decline. The decrease in bare land was mainly converted into urban land, with a smaller proportion transforming into cropland and water bodies. Additionally, some water bodies were converted into cropland, bare land, and urban land. A comparison of LULC changes from 2000 to 2010 and from 2010 to 2020 reveals that, while the total areas of all LULC types experienced only slight changes during the first phase, a more rapid transformation occurred in the second phase. We concluded, that from 2000 to 2020, the entire areas of urban land and water bodies progressively increased, whereas the total areas of cropland, forest land, and bare land declined significantly over the past two decades.

3.4 Evolution of Land-Use Degree

The rate of land use serves as an effective indicator of the extent and intensity of land utilization and growth. Utilizing the LULC information for the YRD, our research assesses various land categories and systematically calculates the evolution of land-use levels to quantify the general amount of land use (2000 – 2020). Figure 6, depicted the spatial dispersal of the evolution of land-use levels. The Land-use levels in the YRD (2000–2020) measures the intensity of human influence on land use patterns.

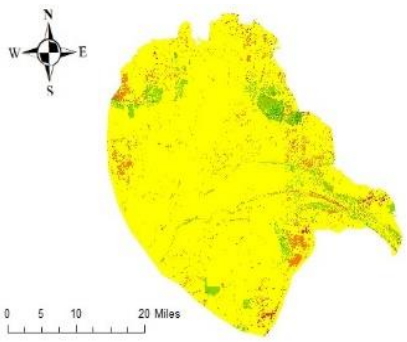

(a). 2000-2010

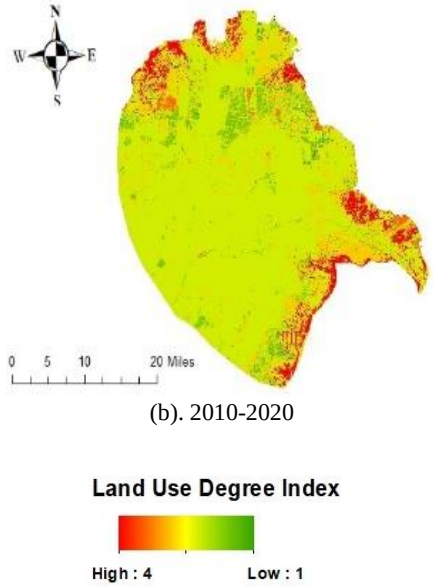

(b). 2010-2020

Figure 6. Spatial Dispersal Maps of Evolution of Land-use Degree in the YRD. (a). 2000-2010; (b). 2010-2020

From 2000 to 2010 moderate land use intensity across much of the delta. This could be areas of mixed agricultural activity, perhaps interspersed with small settlements or less intensive industrial activities, while from 2010 to 2020 there's a noticeable increase in land degree change, especially along the southern coastline and the eastern part of the YRD suggesting an increase in high-intensity land use such as urban expansion or industrial development. Using LULC data, the index captures the spatial dispersal of land use, from natural ecosystems to urbanized and industrial areas. Over the study period, noteworthy land use shifts occurred, from 2000 to 2010 there was ambitious by development, and infrastructure development. Notably, there was a rise in construction land like built-up areas and also in ecological land like water-bodies, while natural environments, such as agricultural lands and bare lands faced varying levels of degradation. This analysis provides valuable insights into the region's socio-economic and ecological dynamics, aiding in the development of sustainable land management strategies.

3.5 Influence Analysis of Detection Factors

The influence detector is utilized to evaluate the descriptive authority of numerous aspects influencing the geographical diversity of land-use strength within the research range. The outcomes are presented in Table 10, Table 11 and Table 12. The values of p for all discovery influences were zero, indicating the nominated influences exert a statistically noteworthy influence on the geographical variation of land-use strength. As a result, these factors can be regarded as key determinants in analyzing spatial diversity. The q-values further illustrate that higher q-values are associated with greater explanatory supremacy of each influence concerning spatial distinction of land-use strength. This suggests that factors with higher q-values have a more substantial influence on land-use strength patterns. As shown in Table 10, Table 11, and Table 12, the q-values for soil type, aspect, and elevation exhibited a gradual decline from 2000 to 2020, indicating a weakening influence of these factors over time. In disparity, the q-values for GDP, and population showed a significant increase, with relatively smaller changes observed for other factors. Overall, the q-values for GDP, populace, temperature, and rainfall were notably higher, signifying that these factors have a strong explanatory power regarding LULC changes in the YRD. These factors are thus identified as the primary drivers of LULC variation in the district. In distinction, the q values of aspect and soil types were continually minor than 0.1, demonstrating that they have slight impression on LULC alteration in the YRD. In summary, the analysis reveals that population, GDP, temperature, and precipitation are the main drivers of land-use variation in the YRD, with elevation, slope, aspect, and soil playing more localized and secondary roles in shaping the region's land-use dynamics. The Geographic Detector's findings suggest that socio-economic factors, particularly population density and economic development, have become increasingly dominant in influencing spatial differentiation in land-use strength over the past two eras.

Table 10. The Values of Impact Factors Influencing Land-use Degree in (2000)

Influence Factors	2000		
	q	p	Sequence
S1	0.252	0	4
S2	0.267	0	3
N1	0.290	0	2
N2	0.305	0	1
N3	0.148	0	5
N4	0.147	0	6
N5	0.015	0	8
N6	0.081	0	7

Table 11. The Values of Impact Factors Influencing Land-use Degree in (2010)

Influence Factors	2010		
	q	p	Sequence
S1	0.442	0	1
S2	0.438	0	2
N1	0.240	0	3
N2	0.193	0	4
N3	0.104	0	5
N4	0.103	0	6
N5	0.012	0	8
N6	0.038	0	7

Table 12. The Values of Impact Factors Influencing Land-use Degree in (2020)

Influence Factors	2020		
	q	p	Sequence
S1	0.401	0	2
S2	0.416	0	1
N1	0.179	0	4
N2	0.180	0	3
N3	0.058	0	6
N4	0.059	0	5
N5	0.018	0	8
N6	0.041	0	7

4. Conclusion

This study, utilizing the GEE cloud framework, applied the RF technique to catalogue land use in the YRD and generated multi-temporal land use dispersal maps for the study area. A transfer matrix was then computed to assess land use variations, followed by the Geodetector method to investigate the potential driving mechanisms behind the LULC intensity in the region. The outcomes reveal that from 2000 to 2020, the dominant land use kinds in the YRD were built-up land, followed by cropland, water bodies, bare land, and forest land. Notably, cropland, forest land, and bare land experienced degradation, while urban land and water bodies expanded. Land use transition analysis showed that cropland and bare land were predominantly converted into urban land and water bodies. In terms of land use strength, high-intensity land use areas were mainly rigorous in the plains, with cropland and urban land being the primary land types. Furthermore, a single-factor detector analysis identified population growth, GDP, temperature, and precipitation as the primary factors driving land use variation. By examining the patterns of land use alteration and its influencing forces in the YRD, this study contributes to a deeper sympathetic of the district's land use dynamics and internal mechanisms. The findings provide valuable data for ecological governance and assist local governments in implementing strategies for rational regional preparation, as well as the synchronized, bearable growth of the social economy and atmosphere.

Acknowledgments

This paper is supported by “The Key Research and Development” Project in Henan Province (No. 241111211100).

References

[1] Liu, J., Kuang, W., Zhang, Z., Xu, X., Qin, Y., Ning, J., . . . Chi, W. Spatiotemporal characteristics, patterns, and causes of land-use changes in China since the late 1980s. Journal of Geographical Sciences, 2014, 24(2), 195-210.

[2] Ojima, D. Global land project: Science plan and implementation strategy: IGBP Secretariat, 2005.

[3] Jones, K. R., Venter, O., Fuller, R. A., Allan, J. R., Maxwell, S. L., Negret, P. J., & Watson, J. E. One-third of global protected land is under intense human pressure. Science, 2018, 360(6390), 788-791.

[4] Homer, C., Dewitz, J., Jin, S., Xian, G., Costello, C., Danielson, P., Stehman, S. Conterminous United States land cover change patterns 2001–2016 from the 2016 national land cover database. ISPRS Journal of Photogrammetry and Remote Sensing, 2020, 162, 184-199.

[5] Stefanski, J., Chaskovskyy, O., & Waske, B. Mapping and monitoring of land use changes in post-Soviet western Ukraine using remote sensing data. Applied Geography, 2014, 55, 155-164.

[6] Abdullah, A. Y. M., Masrur, A., Adnan, M. S. G., Baky, M. A. A., Hassan, Q. K., & Dewan, A. Spatio-temporal patterns of land use/land cover change in the heterogeneous coastal region of Bangladesh between 1990 and 2017. Remote Sensing, 2019, 11(7), 790.

[7] Belay, T., & Mengistu, D. A. Land use and land cover dynamics and drivers in the Muga watershed, Upper Blue Nile basin, Ethiopia. Remote Sensing Applications: Society and Environment, 2019, 15, 100249.

[8] Fan, H., Chen, S., Li, Z., Liu, P., Xu, C., & Yang, X. Assessment of heavy metals in water, sediment and shellfish organisms in typical areas of the Yangtze River Estuary, China. MAR POLLUT BULL, 2020,151, 110864.

[9] Pettorelli, N., Ryan, S., Mueller, T., Bunnefeld, N., Jędrzejewska, B., Lima, M., & Kausrud, K. The Normalized Difference Vegetation Index (NDVI): unforeseen successes in animal ecology. Climate Research, 2011, 46(1), 15-27.

[10] Guo, G., Wu, Z., Xiao, R., Chen, Y., Liu, X., & Zhang, X. Impacts of urban biophysical composition on land surface temperature in urban heat island clusters. Landscape and Urban Planning, 2015, 135, 1-10.

[11] Adam, E., Mutanga, O., Abdel-Rahman, E. M., & Ismail, R. Estimating standing biomass in papyrus (Cyperus papyrus L.) swamp: exploratory of in situ hyperspectral indices and random forest regression. International Journal of Remote Sensing, 2014, 35(2), 693-714.

[12] Houborg, R., & McCabe, M. F. A hybrid training approach for leaf area index estimation via Cubist and random forests machine-learning. ISPRS Journal of Photogrammetry and Remote Sensing, 2018, 135, 173-188.

[13] Chen, B., Xiao, X., Li, X., Pan, L., Doughty, R., Ma, J., . . . Wu, Z. A mangrove forest map of China in 2015: Analysis of time series Landsat 7/8 and Sentinel-1A imagery in Google Earth Engine cloud computing platform. ISPRS Journal of Photogrammetry and Remote Sensing, 2017, 131, 104-120.

[14] Paul, A., Mukherjee, D. P., Das, P., Gangopadhyay, A., Chintha, A. R., & Kundu, S. Improved random forest for classification. IEEE Trans on Image Processing, 2018, 27(8), 4012-4024.

[15] Belgiu, M., & Drăguţ, L. Random forest in remote sensing: A review of applications and future directions. ISPRS journal of photogrammetry and remote sensing, 2016, 114, 24-31.

[16] Guo, L., Chehata, N., Mallet, C., & Boukir, S. Relevance of airborne lidar and multispectral image data for urban scene classification using Random Forests. ISPRS Journal of Photogrammetry and Remote sensing, 2011, 66(1), 56-66.

[17] Zhuang, D., & Liu, J. Study on the model of regional differentiationof land use degree in China. Journal of natural resources, 1997, 12(2), 105-111.

[18] Wu, L., Yang, S., Liu, X., Luo, Y., Zhou, X., & Zhao, H. Response analysis of land use change to the degree of human activities in Beiluo River basin since 1976. Acta Geogr. Sin, 2014, 69(1), 54-63.

[19] Zhang, R., & Lu, J. Multiscale spatiotemporal characteristics and influencing factors of intensive cultivated land use in Yangtze River Economic Belt. Trans. Chin. Soc. Agric. Eng, 2019, 35, 271-278.

[20] Wang, H., Qin, F., Xu, C., Li, B., Guo, L., & Wang, Z. Evaluating the suitability of urban development land with a Geodetector. Ecological Indicators, 2021, 123, 107339.

[21] Su, Y., Li, T., Cheng, S., & Wang, X. Spatial distribution exploration and driving factor identification for soil salinisation based on geodetector models in coastal area. Ecological Engineering, 2020, 156, 105